Available online at www.sciencedirect.com
ScienceDirect
Trans. Nonferrous Met. Soc. China 35(2025) 1032−1044
Transactions of Nonferrous Metals Society of China
www.tnmsc.cn

Simultaneous strengthening and toughening of 2014 Al alloy based on precipitation behavior induced by non-isothermal aging

Peng-wei LI[1], Xin WANG[1], An-hui CAI[1], Hong-zhi ZHOU[1], Xiao-peng LIANG[2], Hui-zhong LI[2]

1. School of Mechanical Engineering, Hunan Institute of Science and Technology, Yueyang 414000, China;
2. School of Materials Science and Engineering, Central South University, Changsha 410083, China

Received 17 August 2023; accepted 25 April 2024

Abstract: Non-isothermal aging (NIA) is a composite heat treatment process that involves heating aging, cooling aging, and complex solute precipitation sequences. The precipitation behavior and the strengthening and toughening mechanisms of the 2014 Al alloy during NIA were studied by employing tensile, fatigue crack growth, hardness, and electronic conductivity tests, as well as high-resolution transmission electron microscopy and scanning electron microscopy. The results show that during NIA, the θ' phase exhibits a complex process of nucleation, nucleation and growth, nucleation and growth and coarsening, growth and coarsening, nucleation and growth, and nucleation. NIA treatment imparts a mixed precipitation characteristic on the alloy, which is manifested as coherent precipitates, including GP zones, θ'' phases, small-sized θ' phases, and semi-coherent or non-coherent precipitates such as large-sized θ' phases and equilibrium θ phases. The simultaneous strengthening and toughening of the NIA-treated 2014 Al alloy is caused by the synergistic effects of the particle-shearing mechanism and Orowan bypassing mechanism.
Key words: 2014 Al alloy; non-isothermal aging; precipitation behavior; strengthening and toughening

1 Introduction

The 2014 Al alloy, which exhibits high specific strength, corrosion resistance, and workability, has become one of the most crucial materials in achieving structural weight reduction and is widely used in the production of high-strength large-scale structural parts in the fields of aerospace, rail transit, and automobiles [1−3]. For most structural materials, it is essential to have both high strength and high toughness [4,5], but there is usually a trade-off between the two properties. Therefore, balancing strength and toughness is a core issue in structural materials research.

It has been reported that grain refinement can provide a synergistic improvement in the strength and toughness of alloys to a certain extent [6−8]. However, grain refinement is often achieved through severe plastic deformation and involves challenges such as thermal instability and high manufacturing costs [9−11]. Microalloying is another effective way to improve the comprehensive properties of alloys by promoting the aging dynamics [12−15], although the addition of alloying elements changes the overall chemical composition, thereby affecting other properties and increasing the material preparation cycle and cost. Ultimately, optimizing the aging process and adjusting the precipitation behavior and morphology of precipitates is the most direct and effective means to achieve a synergistic improvement in strength and toughness.

Non-isothermal aging (NIA) is a novel method

Corresponding author: Peng-wei LI, Tel: +86-730-8648806, E-mail: mselpw@163.com;
Hui-zhong LI, Tel: +86-731-88830377, E-mail: lhz606@csu.edu.cn
DOI: https://doi.org/10.1016/S1003-6326(24)66732-4

that has recently received considerable attention for optimizing the precipitation characteristics of Al-based alloys [16−20]. PENG et al [16] performed NIA on the 7050 Al alloy to obtain a combination of beneficial mechanical properties and favorable corrosion resistance. ZHAO et al [17] investigated the precipitation behavior of the 7055 Al alloy during NIA and found that secondary precipitation led to an increase in precipitation density and additional strengthening. WANG et al [18] investigated the effect of NIA on the strength and corrosion behavior of an Al−Zn−Mg−Cu alloy and found that the differences in strength and corrosion resistance were related to the evolution of precipitates in grains and grain boundaries. However, it remains unclear whether NIA treatments can provide a synergistic improvement in the strength and toughness of Al−Cu alloys, and it is necessary to determine the evolution of precipitation during NIA, as well as the relationship between precipitates and mechanical properties of the NIA-treated alloy.

NIA is a composite aging process that involves heating aging and cooling aging, going from low temperature to high temperature and then back to low temperature. Thus, each parameter of the precipitation process, such as nucleation barriers, driving force, and diffusion, evolves simultaneously, causing the precipitation sequence of solute atoms to be activated in a complex manner. In the present work, the precipitation behavior of the 2014 Al alloy during NIA is investigated, focusing on the interaction between precipitates and dislocations under the action of static and dynamic loads to reveal the strengthening and toughening mechanism of the NIA-treated 2014 Al alloy.

2 Experimental

Herein, as-forged 2014 Al with a composition of 4.4% Cu, 0.7% Mg, 0.64% Si, 0.52% Mn, and 0.12% Fe was used. Samples were solution-treated at 510 °C for 1 h and immediately quenched in water, followed by T6 (i.e., isothermal aging) or NIA treatments. During the T6 treatment, samples were heated to 170 °C and held for different time. For the NIA treatment, samples were heated from 25 to 210 °C with a heating rate of 20 °C/h, then cooled to various ending temperatures with a cooling rate of 20 °C/h, and followed by water quenching to obtain different aging degrees. The as-quenched samples heated to 170 °C, heated to 210 °C, and cooled to 140 °C were marked as NIA-H170, NIA-H210, and NIA-C140, respectively. The schematic diagram of the NIA process is shown in Fig. 1.

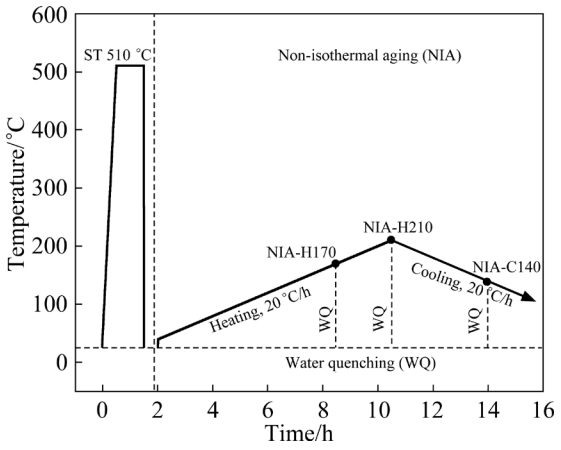

Fig. 1 Schematic diagram of solution treatment (ST) and NIA treatment processes

Microhardness measurements were performed using an HVS−10 Vickers hardness tester (Yanrun Light Machine Technology Co. Ltd., China) with a load of 1 kg and a loading time of 15 s. At least five microhardness measurements were performed on each specimen and then averaged. Electrical conductivity was measured at room temperature using a D60K digital test instrument (Desisen Electronics Co. Ltd., China). To ensure the reliability of the data, at least three measurements were conducted for each specimen. Tensile and fatigue crack propagation (FCP) tests were all conducted on an MTS 810 testing machine (MTS Systems Corporation, USA) according to the GB/T 228.1—2010 and GB/T 6398—2000 standards. The tensile tests were performed with an axial loading speed of 1 mm/min. The FCP tests were conducted on compact tension samples using sinusoidal waveform loading with a stress ratio of 0.1 and loading frequency of 10 Hz. FCP rates were measured under an increasing applied stress intensity factor range, ΔK. The geometry and dimensions of the specimens used for the tensile and FCP tests are shown in Fig. 2.

Microstructural and fractographic tests of the samples were conducted by scanning electron microscopy (SEM, FEI Quanta 200, USA). The characterization of precipitates was performed by

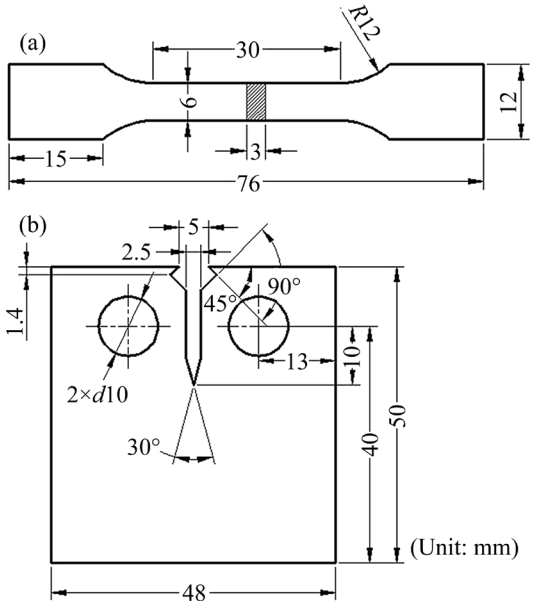

Fig. 2 Geometry and dimensions of specimens used for tensile (a) and FCP (b) tests

high-resolution transmission electron microscopy (HRTEM, FEI Tecnai G2 F20 S-Twin, USA). HRTEM foils were prepared after mechanical grinding to 0.08 mm, followed by twin-jet electrical polishing in a mixture of 30% nitric acid and 70% methanol at 25 V and −30 °C.

3 Results and analysis

3.1 Precipitation behavior in isothermal and non-isothermal aging process

Figure 3 shows the TEM images of the T6-treated samples, as well as the corresponding selected area electron diffraction (SAED) patterns taken from [001] zone axes. As seen in Fig. 3(a), after aging for 2 h, there are a small number of strip-like precipitated phases along the $[\bar{1}00]$ direction and a small amount of point-like precipitated phases in the matrix. In the SAED pattern, in addition to the bright diffraction spots of the α(Al) matrix, there are tiny diffraction spots in the form of crosses around the $\{110\}_\alpha$ forbidden reflections, which are the chief features of the θ' phase commonly found in Al−Cu−Mg−Si alloys [21]. Furthermore, the weakly diffracted streaks through the $\{200\}_\alpha$ planes along the [100] directions correspond to the diffraction feature of the Guinier–Preston (GP) zone or θ'' phase. The weak diffraction spots at $(110)_\alpha$ in the SAED pattern indicate that the point-like precipitates in the matrix are Q phases [22]. When the aging time is extended to 6 h, as shown in Fig. 3(b), the number

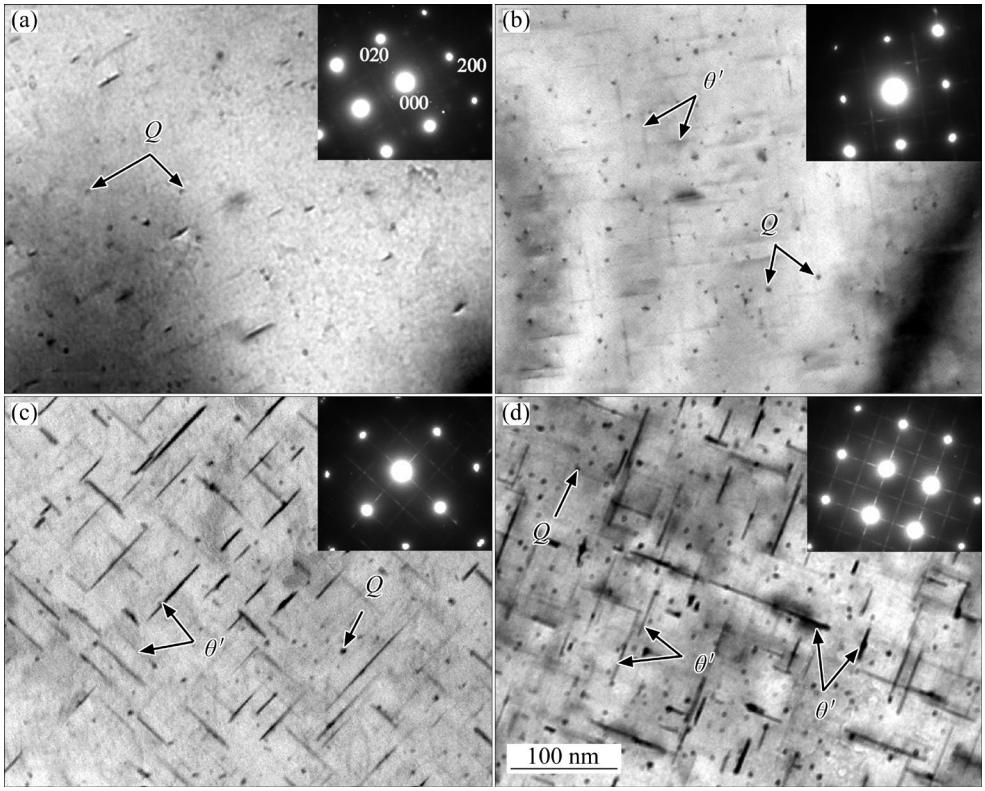

Fig. 3 TEM micrographs and corresponding diffraction patterns of T6-treated samples with aging time of 2 h (a), 6 h (b), 16 h (c), and 38 h (d)

of θ' phases distributed along both the [$\bar{1}$00] and [010] directions increase significantly, and the size increases correspondingly, with a length of 20−50 nm and thickness of 1−2 nm. The number of point-like Q phases also increases. Moreover, the cross-distributed streaks near $(110)_\alpha$ are more distinct, whereas the streaks in the {200} direction become discontinuous, which indicates that the GP zones or θ'' phases mostly transform into θ' phases. After 16 h of aging (i.e., the peak-aging state), as shown in Fig. 3(c), the thickness of the θ' phase increases to 3−5 nm, and the volume fraction begins to decline. When the aging time is extended to 38 h, it can be seen from Fig. 3(d) that part of the θ' phases are coarsened, reaching approximately 7 nm in thickness. The number and size of the Q phases also increase significantly, indicating that the alloy is over-aged, and the metastable θ' phases transform into equilibrium θ phases.

According to the precipitation characteristics observed during the isothermal aging process, there are mainly two types of aging precipitates in the 2014 aluminum alloy, namely the vertically distributed θ' phase and point-like Q phase. Because the Q phase has a hexagonal crystal structure and is very small in size, with a diameter of approximately 1 nm, it causes a small degree of lattice strain on the matrix and has a limited contribution to the strength of the alloy [23]. Therefore, when θ' and Q phases exist simultaneously in the matrix, the θ' phase is the main strengthening phase. Thus, the precipitation characteristics of the θ' phase are discussed only.

Figure 4 shows the curves of microhardness and electrical conductivity for the alloy during the NIA process. In the heating process, the hardness of the alloy increases slightly in the initial stage of aging but gradually decreases in the temperature range of 90−150 °C, and then rapidly increases until reaching the value of HV 153.8 at 210 °C. In contrast, the electrical conductivity increases rapidly throughout the heating process, reaching 36.2% (IACS) at 210 °C. During the subsequent cooling process, the electrical conductivity is continuously increased until it reaches 37.4% (IACS) at 140 °C, after which it remains stable. The hardness decreases slightly during the initial cooling period until the temperature drops below 170 °C and then increases again, reaching a maximum value of HV 162.4 at 140 °C. Subsequently, the hardness gradually decreases again as the temperature continues to decrease.

Figure 5 shows the TEM images and corresponding SAED patterns of the NIA-treated samples. As seen from bright-field TEM images, with the progression of NIA, the volume fraction and size distribution range of the strip-like θ' phases increase. In the SAED pattern of the NIA-H170 sample (Fig. 5(a)), there are relatively weak diffraction spots for the θ' phase along the $[010]_\alpha$ and $[100]_\alpha$ directions and weak streaks along the {200} direction, indicating that there are a large number of GP zones or θ'' phases in the matrix, in addition to θ' phases. For the NIA-H210 sample (Fig. 5(b)), the diffraction intensity of the θ' phase in the SAED pattern is enhanced, and the diffraction characteristics of the continuous streaks along the {200} direction are interrupted, indicating

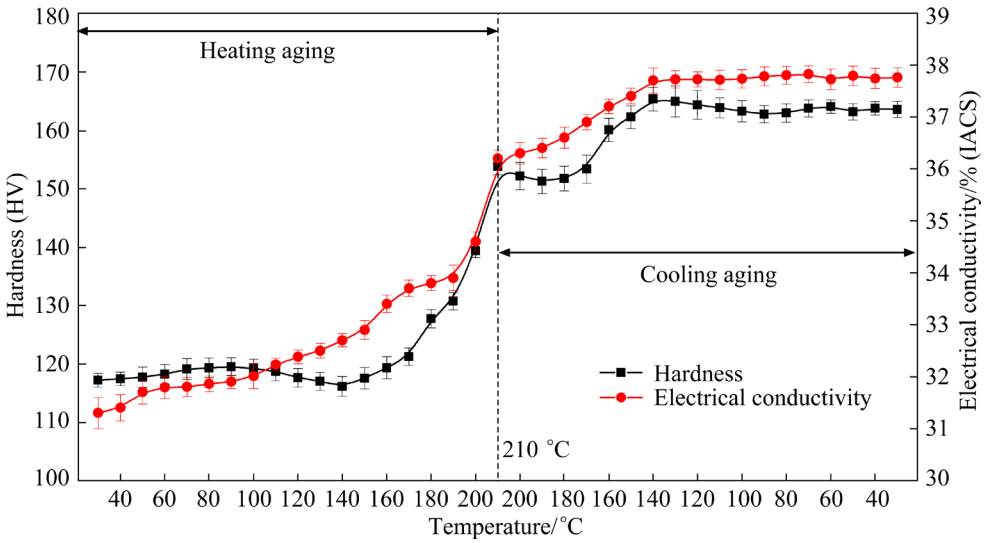

Fig. 4 Microhardness and electrical conductivity of alloy during NIA process

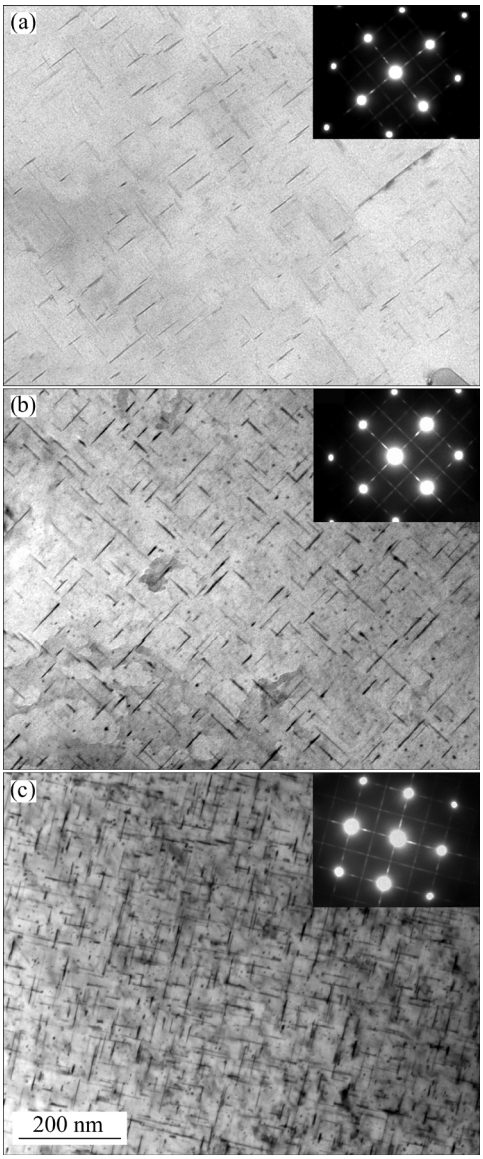

Fig. 5 TEM microstructures of NIA-treated samples: (a) NIA-H170; (b) NIA-H210; (c) NIA-C140

that the GP zones or θ'' phases are reduced and the θ' phase is the main strengthening phase. After cooling aging, the diffraction intensity of the θ' phase in the SAED pattern of the NIA-C140 sample (Fig. 5(c)) is further strengthened, the streaks along the {200} direction are continuous again, and the diffraction intensity is strengthened, indicating that secondary precipitation of the θ' phases and GP zones or θ'' phases occurs during cooling aging.

Figure 6 shows the HRTEM images and the corresponding inverse Fourier transform (IFT) images of the θ' phases of the NIA-C140 sample. As can be seen, the thicknesses of θ' phases are different, among which the smaller size is approximately 2.5−4 nm, and the larger size is approximately 7 nm. The IFT morphology of the smaller θ' phase is the same as that of the Al matrix, while the larger θ' phase overlaps with that of the Al matrix, which indicates that the smaller θ' phase has relatively good congruency with the matrix, while the larger θ' phase has poor congruency with the matrix.

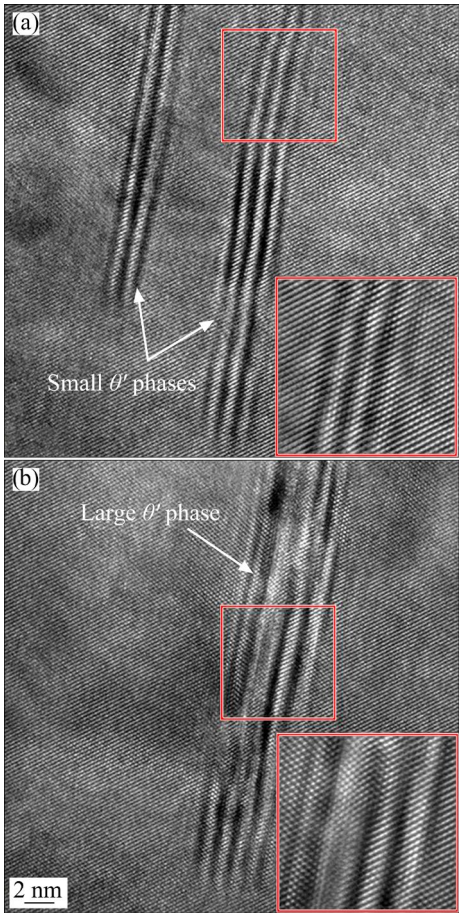

Fig. 6 HRTEM morphologies of small θ' phases (a) and large θ' phase (b) in NIA-C140 sample

During isothermal aging, the precipitation of θ' phase strictly follows the three stages of nucleation, growth, and coarsening [24]. In the nucleation stage, Cu atoms are constantly precipitated from the supersaturated solid solution to form GP zones, which gradually change into ordered θ'' phases. With aging, Cu atoms continue to segregate, and the GP zones and θ'' phases begin to transform into θ' phases and enter into the growth stage. In this process, the amount of precipitated phase remains unchanged, and its size gradually increases until it reaches the peak-aging state. In the coarsening stage, adjacent θ' phases with different sizes have a concentration gradient because of the different Cu contents, and the Cu atoms migrate from the small θ'

phase to the large θ' phase, resulting in coarsening and the formation of an equilibrium θ phase, which leads to the decrease in the precipitate density. Therefore, θ' phases are the main precipitates in the T6-aged alloy.

In the heating process of NIA, with the linear increase in temperature, Cu atoms in the supersaturated solid solution begin to dissolve and nucleate at positions of high energy in the matrix, forming GP zones that are completely congruent with the matrix and disperse easily, causing lattice distortion and increasing the strength of the alloy. However, owing to the small size of the GP zone, its strengthening effect is not significant. Moreover, with the precipitation of Cu atoms, the solid solution strengthening effect gradually decreases. Therefore, in the initial stage of heating aging, the hardness of the alloy increases slowly. With the increase in temperature, nucleation begins in the locations where it is difficult to nucleate at low temperatures, but not all nucleation cores can exist stably. Some unstable nucleation cores dissolve into the matrix again and only stable nucleation cores can continue to grow. Therefore, in this process, the nucleation of the GP zone, the growth of the θ'' phase, and the redissolution of the GP zone occur simultaneously. The strengthening caused by the nucleation of the initial θ'' phase cannot make up for the softening caused by the dissolution of the GP zone, so the hardness of the alloy decreases slightly. With the continuous increase in temperature, the θ'' phase continues to nucleate and grow and even transforms into the θ' phase, so the hardness of the alloy increases. Therefore, the nucleation, growth, and coarsening of the θ' phase occur at the same time during heating.

In the subsequent cooling process of NIA, owing to the high temperature at the initial stage, the θ' phases that preferentially nucleated and grew in the heating process begin to coarsen, whereas the small-sized θ' phases that nucleated and grew later in the heating process continue to grow. Therefore, the growth and coarsening of the θ' phase occur simultaneously at the early stage of cooling aging, and the strengthening caused by the growth of the small θ' phase counteracts the softening caused by the coarsening of the large θ' phases. Thus, the hardness remains relatively stable or decreases slightly. As the temperature decreases, the diffusion of Cu atoms decreases, and the coarsening of θ' phases is restrained, but the growth of θ' phases is continued. When the temperature drops to approximately 170 °C, the Cu atoms, which dissolved back into the matrix because of the instability of the nucleation core, precipitate again and gradually nucleate and grow. Thus, the nucleation and growth of the θ' phase occur simultaneously at this stage, and the hardness of the alloy increases again. With a further decrease in temperature, the growth of θ' phase is inhibited, but the precipitation of GP zones or the growth of θ'' phases continues until reaching the maximum precipitation of Cu atoms.

The electrical conductivity of the alloy increases continuously during the whole NIA process, even during cooling aging, suggesting that secondary precipitation occurs during the cooling process of NIA [25]. Furthermore, the change in the rate of increase for electrical conductivity at different temperature stages is indicative of the different precipitation behavior [26]. Nucleation is the main precipitation behavior in the early stage of heating aging. Because the GP zone or θ'' phase is completely coherent with the matrix, its scattering effect on electrons is still strong, so the electrical conductivity changes relatively slowly. With the linear increase in temperature, the nucleation, growth, and coarsening of precipitates occur at the same time, and the coherent relationship between precipitates and the matrix becomes worse. As a result, the scattering of electrons is reduced, and the electrical conductivity is rapidly increased. In the subsequent cooling aging process, owing to the high temperature at the initial stage, the θ' phase is in a state of growth and coarsening. With the decrease in temperature, the coarsening of θ' phases is inhibited, and the redissolved GP zone nucleates again and gradually transforms into θ'' and θ' phases, increasing the content of the coherent precipitates in the matrix. Therefore, compared with the heating process, the electrical conductivity growth rate decreases in the cooling process. Moreover, with a further decrease in temperature, the diffusion of Cu atoms is inhibited, the precipitation behavior remains in the nucleation stage, and the electrical conductivity of the alloy gradually becomes stable.

Consequently, throughout the whole NIA process, the precipitation of the θ' phase undergoes a complex process of nucleation, nucleation and

growth, nucleation and growth and coarsening, growth and coarsening, nucleation and growth, and finally nucleation. As a result, in addition to θ' phases, GP zones and θ'' phases are mixed in the matrix of non-isothermal-aged alloy.

3.2 Quasi-static and dynamic mechanical properties

Figure 7 shows the quasi-static tensile properties of T6 and NIA-C140 samples at room temperature. As illustrated in Fig. 7(a), the tensile properties of the NIA-C140 samples are enhanced compared with those of the T6 samples. The yield strength (YS), ultimate tensile strength (UTS), and elongation (El) of the NIA-C140 sample are 458.8 MPa, 521.7 MPa, and 12.5%, respectively. Notably, the strength and ductility of the NIA sample are simultaneously improved. The toughness of the composite can be estimated from the energy absorption during tensile deformation, which is estimated by integrating the area under the stress−strain curve [27]. Hence, the NIA-C140 sample shows higher toughness. The work-hardening behaviors of the T6 and NIA-C140 samples during tensile tests are analyzed based on the work-hardening rate (i.e., $\theta=\mathrm{d}\sigma/\mathrm{d}\varepsilon$). As illustrated in Fig. 7(b), the work-hardening rate of the T6 sample is higher than that of the NIA-C140 sample.

Figure 8 shows the tensile fracture surfaces of T6 and NIA-C140 samples. The fracture surfaces of

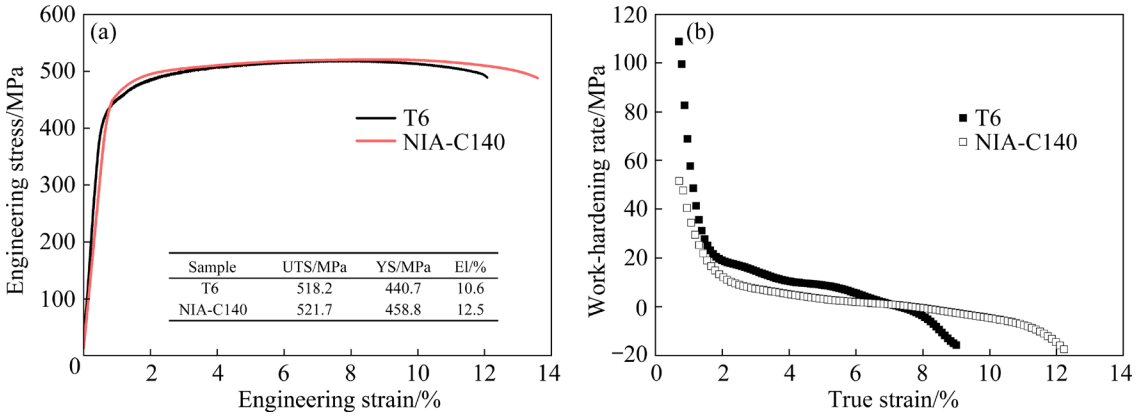

Fig. 7 Mechanical properties of T6 and NIA-C140 samples: (a) Tensile properties; (b) Work-hardening rates

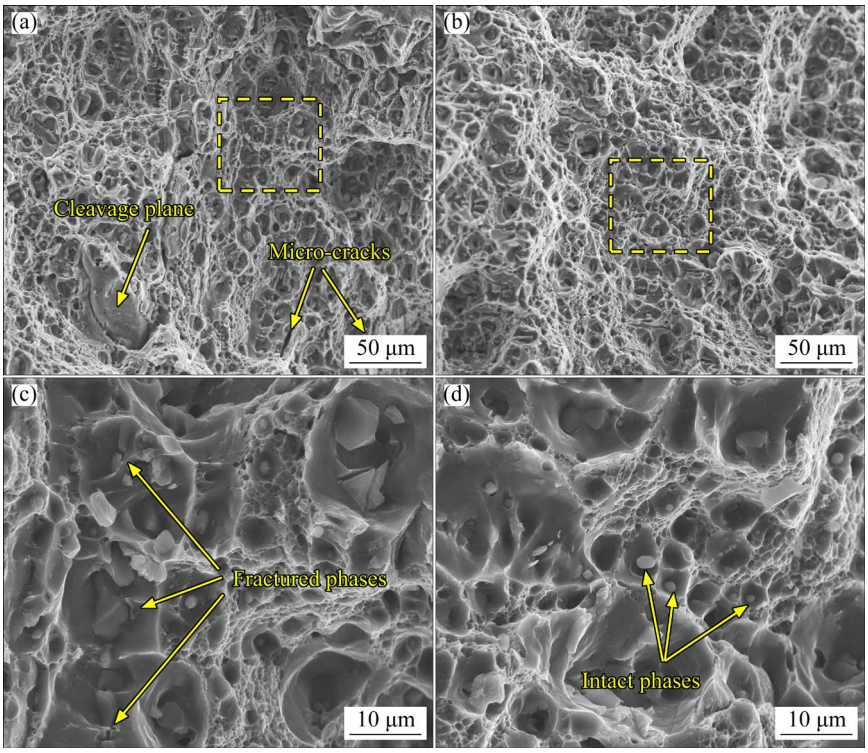

Fig. 8 Tensile fracture morphologies of T6 sample (a, c) and NIA-C140 sample (b, d)

of both samples are covered with many dimples, revealing typical ductile fracture characteristics. The difference is that the fracture of the T6 sample contains a small number of cleavage planes and micro-cracks, and the dimples in the T6 sample are smaller and shallower than those in the NIA sample, suggesting that large local plastic deformation takes place during the tensile test, corresponding to the higher El in the NIA sample. Meanwhile, broken precipitates are observed in the fracture surface of the T6 sample, whereas fewer fractured precipitates are found for the NIA-C140 sample.

Figure 9 shows the FCP curves of the T6 and NIA-C140 samples under cyclic loading. Three typical stages of FCP are observed, from the threshold regime through the steady-state regime (Paris regime) to the instability expansion regime. The crack growth rate of the NIA-C140 sample is lower than that of the T6 sample at every stage. Through linear regression fitting of $(\mathrm{d}a/\mathrm{d}N)_i$ and considering the corresponding ΔK_i data in the range of 1×10^{-6}–5×10^{-6} mm/r, the crack growth rate is determined to be 10^{-7} mm/r. Furthermore, the threshold values of the stress intensity factor (ΔK_{th}) for the NIA-C140 and T6 samples are 5.53 and 4.45 MPa·m$^{1/2}$, respectively. The NIA-C140 sample also has a larger Paris regime than that of the T6 sample, due to the higher toughness of the NIA-C140 sample. The crack growth rate in the Paris regime can be expressed by the Paris formula (i.e., $\mathrm{d}a/\mathrm{d}N=c(\Delta K)^m$), where c and m are material parameters. By linear regression of $\mathrm{d}a/\mathrm{d}N$ and ΔK in the Paris regime, the Paris equation of samples T6 and NIA-C140 is $\mathrm{d}a/\mathrm{d}N=1.653\times10^{-8}\,\Delta K^{3.891}$ and $\mathrm{d}a/\mathrm{d}N=5.361\times10^{-8}\,\Delta K^{3.216}$, respectively.

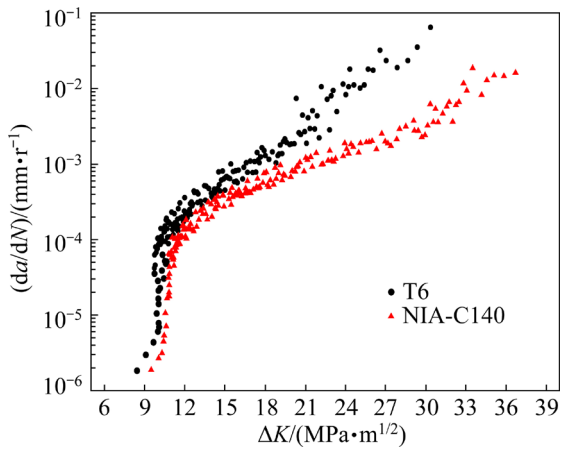

Fig. 9 FCP curves of T6 and NIA-C140 samples

Figure 10 shows the fracture morphologies of the T6 and NIA-C140 samples under the same stress intensity factor range (ΔK=12 MPa·m$^{1/2}$) in the Paris regime. The fracture morphologies of samples with different aging states all show typical crystallographic characteristics, and there are many small facets, tearing edges, and cleavage steps in the fracture. The difference is that the fracture morphology of the T6 sample is rough, the cleavage plane is distinct, and there are secondary cracks along the grain boundary and fatigue steps. From the high-magnification morphology, the spacing of fatigue striations in the NIA-C140 sample is significantly smaller than that in the T6 sample. Using the linear measurement method, it can be roughly determined that the spacing of fatigue striations in the NIA-C140 sample is ~0.15 μm, and that of the T6 sample is ~0.23 μm. By substituting ΔK=12 MPa·m$^{1/2}$ into the corresponding Paris equations, the crack growth rates of NIA-C140 and T6 samples are 0.16 and 0.26 μm/r, respectively, which are consistent with the spacings of the fatigue striations. The average inter-layer spacing of the fatigue striations, which represents a propagation cycle of a fatigue crack [28], indicates that the fatigue crack growth rate of the NIA sample is smaller than that of the T6 sample.

Figure 11 shows the fracture morphologies of the T6 and NIA-C140 samples under the same stress intensity factor range (ΔK=28 MPa·m$^{1/2}$) in the instable expansion regime. The fracture morphologies of samples with different aging states all show typical plastic deformation characteristics, such as dimples and tearing edges. In addition, from the high-magnification images (squared areas in Figs. 11(a, b)), the T6 sample exhibits brittle fracture characteristics such as cleavage facets and intergranular cracks. Conversely, more ductile dimples and tearing ridges are found in the NIA-C140 sample, and the fatigue striations can still be observed in the instable expansion regime. This indicates that under the same stress intensity factor range (ΔK) of 28 MPa·m$^{1/2}$, the T6 sample has entered the stage of complete plastic fracture, whereas the NIA-C140 sample remains in the stage of crack growth. However, under the large stress intensity factor, the crack growth is already unstable, and the crack growth rate is large.

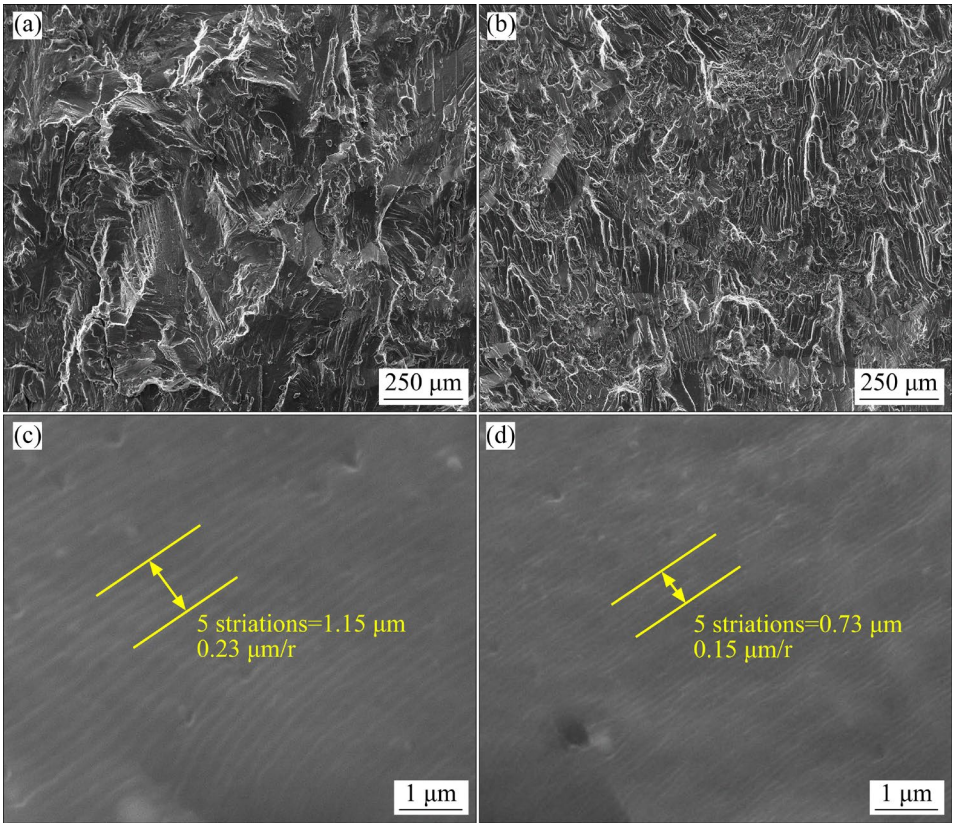

Fig. 10 SEM images in stable crack-growth zone of T6 sample (a, c) and NIA-C140 sample (b, d) under same stress intensity factor range (ΔK) of 12 MPa·m$^{1/2}$

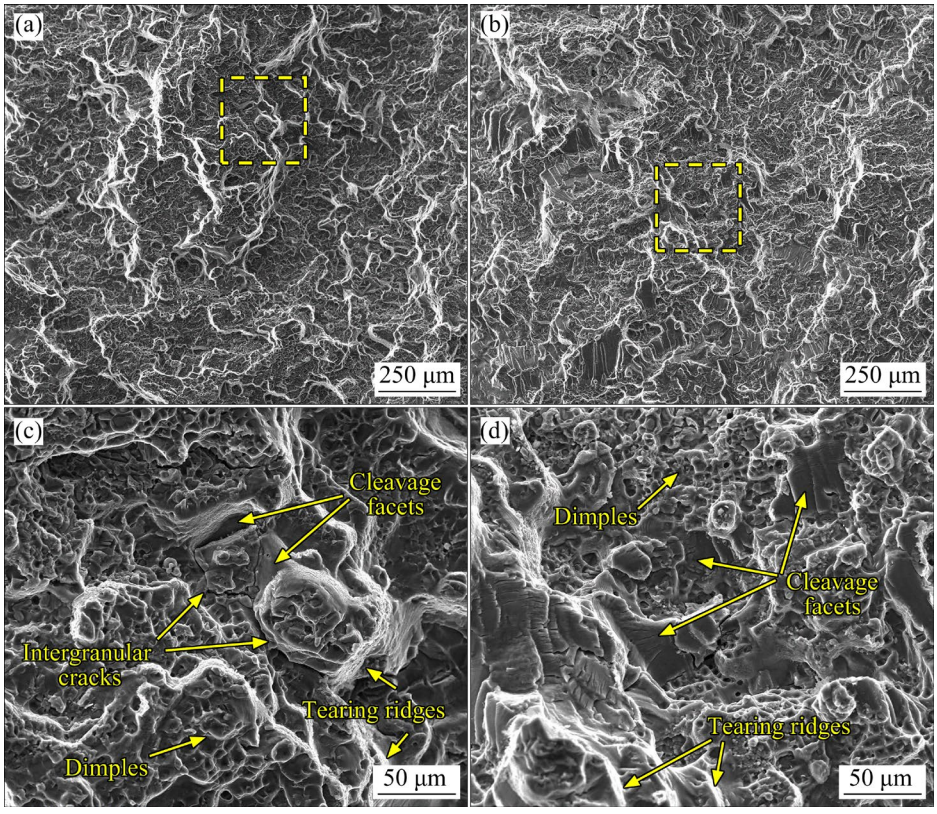

Fig. 11 SEM images in instable crack growth zones in T6 sample (a, c) and NIA-C140 sample (b, d) under same stress intensity factor range (ΔK) of 28 MPa·m$^{1/2}$

3.3 Strengthening and toughening mechanism of non-isothermal aging

For aging-strengthened Al alloys, the type, morphology, quantity, volume fraction, and distribution of precipitates have a direct effect on the physical properties. Precipitates that have congruency with the matrix interact with the dislocations through a particle-shearing mechanism, and their contribution to the strength of the alloy can be expressed as $\sigma=c_A f^m r^n$, where c_A, m and n are constants, f is the volume fraction of precipitates, and r is the radius of precipitates [29]. From the formula, the strength of the alloy can be effectively improved with the increase in the volume fraction and size of the shearable precipitates. Moreover, under the action of the particle-shearing mechanism, dislocations cut through the precipitates and deform them with the matrix, thereby reducing stress concentration, coordinating the deformation, and improving the plasticity and toughness of the alloy.

Dislocations cannot cut through the large θ' phases and equilibrium θ phases with poor matrix coherency, but can only interact with them in a bypassing manner, known as the Orowan bypassing mechanism. Under the bypassing mechanism, the repulsion force of precipitates to dislocations is sufficiently large, causing dislocations to bend and leave dislocation rings around the precipitates. However, the dislocation rings increase the resistance of the precipitates to subsequent passing dislocations, resulting in a strengthening effect. The contribution of the Orowan bypassing mechanism to the strength of the alloy can be expressed as $\Delta\sigma=c_B f^{1/2} r^{-1}$, where c_B is a constant [30]. The strengthening effect is more apparent when the precipitates are smaller. When the size of precipitates is fixed, the strengthening effect is enhanced for larger volume fractions.

For the T6 sample, most of the precipitates are semi-coherent or completely incoherent, and interact with dislocations through the bypassing mechanism, resulting in rapid dislocation proliferation and stress concentration. Therefore, the alloy has high strength but low ductility, which is consistent with the high work-hardening rate. The NIA-treated sample is mixed with precipitates that have different coherency levels, which interact through both the particle-shearing and bypassing mechanisms. The bypassing mechanism ensures the strength of the alloy, and the shearing mechanism reduces the growth rate of dislocations as well as the stress concentration, improving the ductility and toughness of the alloy. Notably, there are many shearable precipitates in the NIA-treated sample, but the strength is higher than that of the T6 sample because of the large precipitation density and high dispersion distribution. Therefore, based on the mixed precipitation characteristics, consisting of shearable GP zones, θ'' phases, and small-sized θ' phases, as well as non-shearable large-sized θ' phases and equilibrium θ phases, the ductility and toughness of the NIA-treated alloy are greatly improved without sacrificing strength.

Stress concentration and slip localization play significant roles in determining the crack growth behavior of Al alloys [31−33]. Stress concentration is caused by the pinning of precipitates to dislocations, whereas slip localization is associated with easy shearing of precipitates by dislocation motion. In the case of cyclic loading, the bypassing mechanism is induced by the interaction between semi-coherent or non-coherent precipitates and the dislocations, and the movement of the dislocations is hindered, which creates a barrier to subsequent dislocation motion. In this case, it is easy to produce alternating slips with multiple slip tracks, resulting in more non-localized slip but irreversible deformation and stress concentration. Consequently, the deformation resistance of the plastic zone at the crack tip is increased, and debonding easily occurs along the interface of precipitates and the matrix [34], resulting in an accelerated crack propagation rate.

In contrast, for the shearing mechanism between coherent precipitates and dislocations, when a dislocation cuts through a precipitate on a certain slip plan, the movement of subsequent dislocations on the same plane becomes easier. Thus, dislocations cut through precipitates and localize in a limited number of slip planes, resulting in slip localization and slip reversibility during cyclic loading. The “reversed” dislocations do not cause damage accumulation in the plastic zone at the crack tip during cyclic loading and do not promote crack propagation, resulting in a lower crack propagation rate. Therefore, the mixed precipitation characteristics of coherent and non-coherent precipitates in NIA samples result in both bypassing and shearing mechanisms under cyclic loading. The bypassing mechanism makes

plastic deformation more uniform at the crack tip and thus improves the crack propagation resistance, while the shearing mechanism promotes slip reversibility and reduces the stress concentration at the crack tip, thus reducing the crack propagation rate.

4 Conclusions

(1) The main strengthening phase of the 2014 Al alloy is the θ' phase. During isothermal aging, precipitation of θ' phases proceeds successively in three stages: nucleation, growth, and coarsening. During NIA, the precipitation of θ' phases undergoes a complex process of nucleation, nucleation and growth, nucleation and growth and coarsening, growth and coarsening, nucleation and growth, and finally nucleation.

(2) NIA imparts mixed precipitation characteristics on the 2014 Al alloy, which is manifested as coherent precipitates, such as GP zones, θ'' phases, and small-sized θ' phases, and semi-coherent or non-coherent precipitates such as large-sized θ' phases and equilibrium θ phases.

(3) Under static or cyclic loading, coherent precipitates interact with dislocations through the particle-shearing mechanism, which coordinates the deformation and reduces the stress concentration, thereby improving the toughness and reducing the crack growth rate. Semi-coherent or non-coherent precipitates interact with dislocations through the bypassing mechanism, which promotes the work-hardening rate and increased strength, as well as the crack initiation resistance.

CRediT authorship contribution statement

Peng-wei LI: Project administration, Funding acquisition, Writing − Review & editing; **Xin WANG:** Investigation, Resources, Writing − Original draft; **An-hui CAI:** Methodology, Writing − Review & editing; **Hong-zhi ZHOU:** Investigation, Supervision, Data curation; **Xiao-peng LIANG:** Visualization, Writing − Review & editing; **Hui-zhong LI:** Methodology, Validation, Supervision.

Declaration of competing interest

The authors declare that they have no known competing financial interests or personal relationships that could have appeared to influence the work reported in this paper.

Acknowledgments

This work was supported by the Science Foundation of Hunan Province, China (No. 2020JJ5215), Scientific Research Project of Hunan Provincial Department of Education, China (No. 21B0594), and the Open Fund of Hunan Key Laboratory of Electromagnetic Equipment Design and Manufacturing, China (No. DC202007).

References

[1] LI Peng-wei, LI Hui-zhong, HUANG Lan, LIANG Xiao-peng, ZHU Ze-xiao. Characterization of hot deformation behavior of AA2014 forging aluminum alloy using processing map [J]. Transactions of Nonferrous Metals Society of China, 2017, 27: 1677−1688.

[2] ARIF M A M, OMAR M Z, SAJURI Z, SALLEH M S. Effects of Cu and Mg on thixoformability and mechanical properties of aluminium alloy AA2014 [J]. Transactions of Nonferrous Metals Society of China, 2020, 30: 275−287.

[3] BABUTSKYI A, MOHIN M, CHRYSANTHOU A, XU Y, LEWIS A. Effect of electropulsing on the fatigue resistance of aluminium alloy AA2014-T6 [J]. Materials Science and Engineering A, 2020, 772: 138679.

[4] SHEN Tong, FAN Cai-he, HU Ze-yi, WU Qin, NI Yu-meng, CHEN Yu-zhou. Effect of strain rate on microstructure and mechanical properties of spray-formed Al−Cu−Mg alloy [J]. Transactions of Nonferrous Metals Society of China, 2022, 32: 1096−1104.

[5] LIU Jian, CHENG Yuan-sheng, CHAN S W N, SUNG D. Microstructure and mechanical properties of 7075 aluminum alloy during complex thixoextrusion [J]. Transactions of Nonferrous Metals Society of China, 2020, 30: 3173−3182.

[6] ZHANG Xin-kui, LI Lie-jun, WANG Zhi, PENG Han-lin, CHEN Song-jun, BAN Tao, GAO Ji-xiang, PENG Zheng-wu. Ultrafine-grained Al−La−Mg−Mn alloy with superior thermal stability and strength−ductility synergy [J]. Materials Science and Engineering A, 2023, 873: 145035.

[7] YANG Bo-wei, GAO Min-qiang, YANG Li, LI Bing, GUAN Ren-guo. Enhancing the strength and ductility in an Al−5Mg alloy via accumulative continuous extrusion forming at room and cryogenic temperatures [J]. Journal of Alloys and Compounds, 2023, 960: 170817.

[8] JIANG Jing-yu, WANG Hui-ling, TONG Meng-meng, JIANG Feng, ZHANG Meng-han. Effect of cryogenic environment on tensile property and microstructure evolution of an Al−Mg−Sc alloy [J]. Materials Characterization, 2023, 195: 112550.

[9] YANG Bo-wei, WANG Yu, GAO Min-qiang, WANG Chang-feng, GUAN Ren-guo. Microstructural evolution and strengthening mechanism of Al−Mg alloys with fine grains processed by accumulative continuous extrusion forming [J]. Journal of Materials Science & Technology, 2022, 128: 195−204.

[10] JIN Shuo-xun, WANG An-ding, WANG Kang, LI Wen-fang, WAN Bing-bing, ZHAI Tong-guang. Significant strengthening effect in ultra-fine grained Al alloy made by

fast solidification and hot extrusion processes [J]. Journal of Materials Research and Technology, 2022, 16: 1761−1769.

[11] FENG Xiu-li, LIU Hui-jie, BABU S S. Effect of grain size refinement and precipitation reactions on strengthening in friction stir processed Al−Cu alloys [J]. Scripta Materialia, 2011, 65: 1057−1060.

[12] ZHANG Ming-xue, WANG Cheng, ZHANG Shao-you, LIU Xu, WANG Xuan, REN Ming-wen, WANG Hui-yuan. Enhanced aging precipitation behavior and mechanical properties of 6022 Al−Mg−Si alloy with Zr addition [J]. Materials Science and Engineering A, 2022, 840: 142957.

[13] WANG Yi-fan, LU Yan-li, XU Jin-han, ZHANG Shi-yao, WU Wei, CHEN Zheng. The effects of Ti on the precipitation evolution and age-hardening behavior of Al−7Si−Mg alloy [J]. Intermetallics, 2022, 148: 107642.

[14] CHEN M C, CHUNG T F, TAI C L, CHEN Y H, YANG J R, LEE S L, HSIAO C N, TSAO C S, CHOU C M. Quantitative evaluation of the effect of Ag-addition on the concurrently-existing precipitation kinetics in the aged Al−Cu−Mg(−Ag) alloys [J]. Materials & Design, 2023, 227: 111766.

[15] KIM Y Y, ROSENTHAL D F T, SHIN D W, SON H W, LEE S H, CHO Y H, SEIDMAN D N, EUH K. Effects of Sn addition on precipitation of Al−Zn−Mg alloy at early stage of natural aging [J]. Journal of Materials Research and Technology, 2023, 26: 697−702.

[16] PENG Xiao-yan, GUO Qi, LIANG Xiao-peng, DENG Ying, GU Yi, XU Guo-fu, YIN Zhi-min. Mechanical properties, corrosion behavior and microstructures of a non-isothermal ageing treated Al−Zn−Mg−Cu alloy [J]. Materials Science and Engineering A, 2017, 688: 146−154.

[17] ZHAO H, YE L Y, CHENG Q S, KANG Y, ZHANG W J. Enhanced mechanical properties and corrosion resistance of 7055 aluminum alloy through variable-rate non-isothermal aging [J]. Journal of Alloys and Compounds, 2023, 943: 169198.

[18] WANG Wei-yi, PAN Qing-lin, WANG Xiang-dong, SUN Yuan-wei, YE Ji, LIN Geng, LIU Shu-hui, HUANG Zhi-qi, XIANG Sheng-qian, WANG Xiao-ping, LIU Ya-ru. Non-isothermal aging: A heat treatment method that simultaneously improves the mechanical properties and corrosion resistance of ultra-high strength Al−Zn−Mg−Cu alloy [J]. Journal of Alloys and Compounds, 2020, 845: 156286.

[19] PENG Xiao-yan, LI Yao, LIANG Xiao-peng, GUO Qi, XU Guo-fu, PENG Yong-yi, YIN Zhi-min. Precipitate behavior and mechanical properties of enhanced solution treated Al−Zn−Mg−Cu alloy during non-isothermal ageing [J]. Journal of Alloys and Compounds, 2018, 735: 964−974.

[20] NICOLAS M, DESCHAMPS A. Characterization and modelling of precipitate evolution in an Al−Zn−Mg alloy during non-isothermal heat treatments [J]. Acta Materialia, 2003, 51: 6077−6094.

[21] RIONNO G, ZANADA A. Coupled formation of hardening particles on pre-precipitates in an Al−Cu−Mg−Si AA2014 alloy [J]. Materials Letters, 1998, 37: 241−245.

[22] BISWAS A, SIEGEL D J, SEIDMAN D N, Compositional evolution of *Q*-phase precipitates in an aluminum alloy [J]. Acta Materialia, 2014, 75: 322−336.

[23] BOBEL A, KIM K, WOLVERTON C, WALKER M, OLSON G B. Equilibrium composition variation of *Q*-phase precipitates in aluminum alloys [J]. Acta Materialia, 2017, 138: 150−156.

[24] SON S K, TAKEDA M, MITOME M. Precipitation behavior of an Al−Cu alloy during isothermal aging at low temperatures [J]. Materials Letters, 2005, 59: 629−632.

[25] KE Bin, YE Ling-ying, ZHANG Yong, LIU Xiao-dong, DONG Yu, WANG Ping, TANG Jian-guo, LIU Sheng-dan. Enhanced strength and electrical conductivities of an Al−Zn−Mg aluminum alloy through a new aging process [J]. Materials Letters, 2021, 304: 130586.

[26] VANDERSLUIS E, RAVINDRAN C, BAMBERGER M. Mechanisms affecting hardness and electrical conductivity in artificially-aged B319 aluminum alloy [J]. Journal of Alloys and Compounds, 2021, 867: 159121.

[27] JIANG L, YANG H, YEE J K, MO X, TOPPING T, LAVERNIA E J, SCHOENUNG J M. Toughening of aluminum matrix nanocomposites via spatial arrays of boron carbide spherical nanoparticles [J]. Acta Materialia, 2016, 103: 128−140.

[28] TIAN D D, LIU X S, HE G Q, SHEN Y, LV S Q, WANG Q G. Low cycle fatigue behavior of casting A319 alloy under two different aging conditions [J]. Materials Science and Engineering A, 2016, 654: 60−68.

[29] CHEN Jun-zhou, ZHEN Liang, YANG Shou-jie, SHAO Wen-zhu, DAI Sheng-long. Investigation of precipitation behavior and related hardening in AA 7055 aluminum alloy [J]. Materials Science and Engineering A, 2009, 500: 32−42.

[30] LIU Yan, JIANG Da-ming, LI Bing-qing, YANG Wen-shu, HU Jie. Effect of cooling aging on microstructure and mechanical properties of an Al−Zn−Mg−Cu alloy [J]. Materials & Design, 2014, 57: 79−86.

[31] HOCKAUF K, WAGNER M F X, HALLE T, NIENDORF T, HOCKAUF M, LAMPKE T. Influence of precipitates on low-cycle fatigue and crack growth behavior in an ultrafine-grained aluminum alloy [J]. Acta Materialia, 2014, 80: 250−263.

[32] HORNBOGEN E, GAHR K H Z. Microstructure and fatigue crack growth in a γ-Fe−Ni−Al alloy [J]. Acta Metallurgica, 1976, 24: 581−592.

[33] GLEITER H, HORNBOGEN E. Precipitation hardening by coherent particles [J]. Materials Science and Engineering, 1968, 2: 285−302.

[34] HAO Hong, YE Du-yi, CHEN Chuan-yong. Strain ratio effects on low-cycle fatigue behavior and deformation microstructure of 2124-T851 aluminum alloy [J]. Materials Science and Engineering A, 2014, 605: 151−159.

基于非等温时效诱导析出行为的 2014 铝合金协同强化与增韧

李鹏伟[1]，王 昕[1]，蔡安辉[1]，周宏志[1]，梁霄鹏[2]，李慧中[2]

1. 湖南理工学院 机械工程学院，岳阳 414000；
2. 中南大学 材料科学与工程学院，长沙 410083

摘 要：非等温时效是一种包括加热时效、冷却时效和复杂溶质析出序列的复合热处理工艺。采用拉伸、疲劳裂纹扩展、硬度、电导率测试以及 HRTEM 和 SEM 对 2014 铝合金在非等温时效过程中的析出行为和强化增韧机制进行研究。结果表明：在非等温时效过程中，θ'相的析出先后经历形核、形核+长大、形核+长大+粗化、长大+粗化、形核+长大、形核的复杂过程。非等温时效使合金具有混合析出相的特点，主要表现为以 GP 区、θ''相、小尺寸 θ'相为主的共格析出相和以大尺寸 θ'相、平衡 θ 相为主的非共格析出相。非等温时效态 2014 铝合金的强韧化是析出相与位错间的粒子切过机制和 Orowan 绕过机制协同作用的结果。

关键词：2014 铝合金；非等温时效；析出行为；强韧化

(Edited by Bing YANG)